Inorganic Chemistry

Article

pubs.acs.org/IC

Four New Three-Dimensional Polyoxometalate-Based Metal–Organic Frameworks Constructed From $[Mo_6O_{18}(O_3AsPh)_2]^{4-}$ Polyoxoanions and Copper(I)-Organic Fragments: Syntheses, Structures, Electrochemistry, and Photocatalysis Properties

Bo Liu,[†,§] Jin Yang,*[,†] Guo-Cheng Yang,[‡] and Jian-Fang Ma*[,†]

[†]Key Lab of Polyoxometalate Science, Department of Chemistry, Northeast Normal University, Changchun 130024, People's Republic of China

[‡]School of Chemistry and Life Science, Changchun University of Technology, Changchun 130012, People's Republic of China

[§]Department of Chemistry, Jilin Normal University, Siping 136000, People's Republic of China

Supporting Information

ABSTRACT: Four novel polyoxometalate-based copper(I)-organic frameworks, namely, $[Cu^I_2(cis\text{-}L1)_2][Cu^I_2(trans\text{-}L1)_2Mo_6O_{18}(O_3AsPh)_2]$ (**1**), $[Cu^I_4(L2)_4Mo_6O_{18}(O_3AsPh)_2]$ (**2**), $[Cu^I_4(L3)_4Mo_6O_{18}(O_3AsPh)_2]$ (**3**), and $[Cu^I_4(L4)_2Mo_6O_{18}(O_3AsPh)_2]$ (**4**) (L1 = 1,3-bis(1,2,4-triazol-1-yl)propane, L2 = 1,4-bis(1,2,4-triazol-1-yl)butane, L3 = 1,5-bis(1,2,4-triazol-1-yl)pentane, and L4 = 1,6-bis(1,2,4-triazol-1-yl)hexane), have been successfully synthesized under hydrothermal conditions. Their structures have been determined by single-crystal X-ray diffraction analyses and further characterized by elemental analyses, infrared spectra (IR), UV–vis spectra, powder X-ray diffraction (PXRD), and thermogravimetric (TG) analyses. Compound **1** is composed of two crystallographically independent and distinct polymeric motifs: one-dimensional (1D) S-shaped chain and two-dimensional (2D) undulated layer. The S-shaped chains penetrated into the 2D parallel layers to generate an unusual 1D + 2D → three-dimensional (3D) poly*pseudo*-rotaxane framework. In **2**, the As_2Mo_6 polyoxoanions in tetradentate modes link four neighboring –L2–Cu–L2– chains to produce a rare 3D trinodal (3,4)-connected self-penetrated framework with Point Symbol of $(8^3)_2(8^2{\cdot}12^4)$. In **3**, adjacent Cu^I atoms are linked by As_2Mo_6 polyoxoanions and L3 ligands into a 2D layer. The layers are further interlocked by the two nearest neighboring ones to form a 3D polycatenated framework. In **4**, L4 ligands bridge four Cu^I atoms to yield 2D wavelike layers, which are further linked by the octadentate As_2Mo_6 polyoxoanions to form a 3D tetranodal (3,4,6)-connected framework with Point Symbol of $(6^3)(4{\cdot}6^3{\cdot}8^2)(6^4{\cdot}8^2)(4^2{\cdot}6^2{\cdot}8^{10}{\cdot}10)$. In addition, the photocatalytic activities of compounds **1**, **3**, and **4** for decomposition of methylene blue (**MB**) under UV light have been investigated. Moreover, their electrochemical properties have also been studied in 1 M H_2SO_4 aqueous solution.

INTRODUCTION

Polyoxometalates (POMs) are metal-oxide clusters of early transition metals Mo, W, V, and so forth.[1−3] The interest in POM systems stems from their application in various areas, including structural chemistry, analytical chemistry, surface chemistry, medicine, electrochemistry, and photochemistry.[2] In recent years, the introduction of metal–organic frameworks (MOFs) into the POM systems has been emerging as one of the most promising strategies for optimizing the performance of POMs.[3−5] As a result, a large number of examples of POM-based MOFs (PMOFs) have been reported and shown appealing structural motifs with improved properties.[6] So far, most of PMOFs are based on classical POMs. For example, α-$[Mo_8O_{26}]^{4-}$ has widely been investigated and produced a number of charming entangled PMOFs.[3c] However, its analogue $[Mo_6O_{18}(O_3AsPh)_2]^{4-}$ with covalently linked organic groups has received less attention.[2e]

Recently, the flexible N-donor bridging bis(triazole) ligands have shown excellent features in the construction of PMOFs.[6c,7] Compared with rigid 4,4′-bipyridine, their flexibility and conformational freedom allow them to better conform to the coordination environments of the metal cations and POMs. Besides, bis(triazole) ligands have more multiple coordination sites than flexible bis(imidazole) ligands, and therefore, they can adopt more versatile conformations.[8] Thus, the bis-(triazole) ligands are good candidates for the construction of entangled PMOFs.[7,8] In this work, four fascinating PMOFs based on $[Mo_6O_{18}(O_3AsPh)_2]^{4-}$ polyoxoanions and copper(I)-organic fragments, namely, $[Cu^I_2(cis\text{-}L1)_2][Cu^I_2(trans\text{-}L1)_2Mo_6O_{18}(O_3AsPh)_2]$ (**1**), $[Cu^I_4(L2)_4Mo_6O_{18}(O_3AsPh)_2]$ (**2**), $[Cu^I_4(L3)_4Mo_6O_{18}(O_3AsPh)_2]$ (**3**), and

Received: June 13, 2012
Published: December 20, 2012

$[Cu^{I}_4(L4)_2Mo_6O_{18}(O_3AsPh)_2]$ (**4**), where L1 = 1,3-bis(1,2,4-triazol-1-yl)propane, L2 = 1,4-bis(1,2,4-triazol-1-yl)butane, L3 = 1,5-bis(1,2,4-triazol-1-yl)pentane and L4 = 1,6-bis(1,2,4-triazol-1-yl)hexane (Scheme 1), have been successfully synthesized under hydrothermal conditions. The compounds were characterized by IR spectra, UV−vis spectra, TGA, and powder XRD patterns. Photocatalytic activities for dye degradation under UV light irradiation have been studied for compounds **1**, **3**, **4**. In addition, the electrochemical properties of compounds **1**, **3**, and **4** have also been investigated.

Scheme 1. Bis(triazole) Ligands Used In This Work

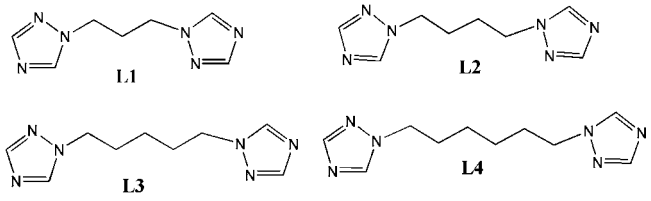

EXPERIMENTAL SECTION

Materials and Instruments. The organic ligands L1−L4 were synthesized by the general method described in the literature.[9] Other reagents were purchased from commercial sources and used as received. Elemental analyses (C, H, and N) were conducted on a Perkin-Elmer 2400CHN elemental analyzer. The inductively coupled plasma (ICP) analyses were performed on a Leeman Laboratories Prodigy inductively coupled plasma-optical atomic emission spectrometer (ICP-AES). The FT-IR spectra were recorded from KBr pellet in the range 4000−400 cm^{-1} on a Mattson Alpha-Centauri spectrometer. The solid diffuse reflectance UV−vis spectra were recorded on a Varian Cary 500 UV−vis spectrometer, whereas the UV−vis spectra for solution samples were obtained on a Shimadzu UV 2450 spectrometer. The powder X-ray diffraction (PXRD) data were collected on a Rigaku RINT2000 diffractometer at room temperature with Cu K_α radiation. Thermogravimetric analyses (TGA) were performed on a Perkin-Elmer TG-7 analyzer heated from room temperature to 800 °C under nitrogen gas. Photocatalytic experiments in aqueous solutions were performed in a 500 mL water-cooled quartz cylindrical vessel. Typically, the reaction mixture in the vessel was maintained at room temperature by a continuous flow of water through an external cooling coil. A 125 W high-pressure mercury lamp was used as the UV light source. To establish an adsorption/desorption equilibrium of methylene blue (**MB**) on the sample surface, a suspension of powdered catalyst (70 mg) in fresh aqueous solution of **MB** (200 mL, 5.0×10^{-5} mol L^{-1}) was magnetically stirred in the dark for 30 min in the vessel before irradiation. At given irradiation time intervals, a series of aqueous solutions of a certain volume were collected and separated through a centrifuge to remove suspended catalyst particles and then subjected to UV−vis spectroscopic measurement. The organic dye concentration was estimated by the absorbance at 665 nm.

X-ray Crystallography. Single-crystal X-ray diffraction data for **1**−**4** were recorded on an Oxford Diffraction Gemini R CCD with graphite-monochromated Mo Kα radiation (λ = 0.71073 Å) at 298 K. The structure was solved by the Direct Method of SHELXS-97[10] and refined by full-matrix least-squares techniques using the SHELXL-97 program[11] within WINGX.[12] Non-hydrogen atoms were refined with anisotropic temperature parameters, and hydrogen atoms of the organic components were refined as rigid groups. The disordered C atoms in compound **2** (C3, C3′ C4, C4′, C15, C15′, C16 and C16′) and **3** (C4, C4′, C5, C5′, C15, C15′, C16, and C16′) were refined using C atoms split over two sites, with a total occupancy of 1. The detailed crystallographic data and structure refinement parameters for these compounds are summarized in Table 1. Selected bond distances and angles are listed in and Supporting Information, Table S1−S4.

Preparations of 1-, 3-, and 4-CPEs. Compound **1** modified carbon paste electrode (**1**-CPE) was fabricated as follows: 90 mg of graphite powder and 9 mg of **1** were mixed and ground together with an agate mortar and pestle to achieve a uniform mixture, and then 0.1 mL of Nujol was added with stirring. The homogenized mixture was packed into a glass tube with a 1.5 mm inner diameter, and the tube surface was wiped with paper. Electrical contact was established with a copper rod through the back of the electrode. **3**- and **4**-CPEs also can be made successfully in a similar manner.

Synthesis of $[Cu^{I}_2(cis\text{-}L1)_2][Cu^{I}_2(trans\text{-}L1)_2Mo_6O_{18}(O_3AsPh)_2]$ 1. A mixture of $Cu(OAc)_2{\cdot}H_2O$ (100 mg, 0.5 mmol), L1 (90 mg, 0.5 mmol), $Na_2MoO_4{\cdot}2H_2O$ (242 mg, 1 mmol), $PhAsO_3H_2$ (200 mg, 1 mol), and water (10 mL) was placed in a 18 mL Teflon reactor. The pH value of the mixture was adjusted to about 3−4 by 4 M HCl, and kept under autogenous pressure at 170 °C for 5 days. Then the mixture was cooled to room temperature, and yellow crystals of **1** were obtained in a 28% yield based on Cu. Elemental analysis results for $C_{20}H_{25}AsCu_2Mo_3N_{12}O_{12}$: Calcd (%): C 21.54, H 2.26, N 15.07, Cu 11.40, Mo 25.81; Found (%): C 21.45, H 2.29, N 15.14; Cu 11.59, Mo 25.60. FTIR (KBr pellet, cm^{-1}): 1527(m), 1475(s), 1448(s), 1278(m), 1213(m), 1144(m), 1094(s), 913(w), 788(w), 633(w), 575(m), 512(m).

Table 1. Crystal Data and Structure Refinements for Compounds 1−4

	1	2	3	4
formula	$C_{20}H_{25}AsCu_2Mo_3N_{12}O_{12}$	$C_{22}H_{29}AsCu_2Mo_3N_{12}O_{12}$	$C_{24}H_{33}AsCu_2Mo_3N_{12}O_{12}$	$C_{16}H_{21}AsCu_2Mo_3N_6O_{12}$
Fw	1115.16	1143.39	1171.44	979.06
crystal system	monoclinic	triclinic	triclinic	monoclinic
space group	$P2_1/c$	$P\bar{1}$	$P\bar{1}$	$P2_1/c$
a [Å]	14.3901(4)	11.3976(3)	11.4894(3)	11.4377(2)
b [Å]	12.5772(4)	13.3822(4)	13.0862(3)	19.3351(3)
c [Å]	21.7574(8)	13.3964(5)	13.1470(3)	14.3898(4)
α [deg]	90	109.716(3)	82.996(2)	90
β [deg]	124.537(2)	96.413(2)	82.647(2)	128.4860(10)
γ [deg]	90	107.931(2)	85.451(2)	90
V [$Å^3$]	3243.81(18)	1776.28(1)	1941.72(8)	2490.97(9)
Z	4	2	2	4
D_c (g/cm^3)	2.283	2.138	2.004	2.611
GOF	0.905	1.052	0.943	0.946
R_{int}	0.0263	0.0191	0.0278	0.0201
$R1$ [$I > 2\sigma(I)$]	0.0247	0.0380	0.0425	0.0224
$wR2$ (all data)	0.0489	0.1092	0.1116	0.0487

dx.doi.org/10.1021/ic301257k | Inorg. Chem. 2013, 52, 84−94

Synthesis of $[Cu^{I}_4(L2)_4Mo_6O_{18}(O_3AsPh)_2]$ 2. Compound **2** was prepared similar to that of compound **1**, but the L2 (95 mg, 0.5 mmol) was used instead of L1. Yellow crystals of **2** were obtained in a 5% yield based on Cu. Elemental analysis results for $C_{22}H_{29}AsCu_2Mo_3N_{12}O_{12}$: Calcd (%): C 23.11, H 2.56, N 14.70, Cu 11.12, Mo 25.17; Found (%): C 23.17, H 2.52, N 14.64, Cu 10.83, Mo 25.29. FTIR (KBr pellet, cm^{-1}): 1529(m), 1473(s), 1438(s), 1279(m), 1212(m), 1136(m), 1090(s), 1004(s), 906(w), 791(w), 658(w), 584(m), 517(m).

Synthesis of $[Cu^{I}_4(L3)_4Mo_6O_{18}(O_3AsPh)_2]$ 3. Compound **3** was prepared similar to that of compound **1**, but the L3 (103 mg, 0.5 mmol) was used instead of L1. Brown crystals of **3** were obtained in a 35% yield based on Cu. Elemental analysis results for $C_{24}H_{33}AsCu_2Mo_3N_{12}O_{12}$: Calcd (%): C 24.61, H 2.84, N 14.35, Cu 10.85, Mo 24.57; Found (%): C 24.56, H 2.87, N 14.29, Cu 10.73, Mo 24.69. FTIR (KBr pellet, cm^{-1}): 1525(s), 1476(s), 1436(m), 1297(m), 1209(s), 1136(m), 1092(m), 995(s), 948(w), 887(w), 791(w), 648(w), 583(m), 518(m).

Synthesis of $[Cu^{I}_4(L4)_2Mo_6O_{18}(O_3AsPh)_2]$ 4. Compound **4** was prepared similar to that of compound **1**, but the L4 (110 mg, 0.5 mmol) was used instead of L1. Brown crystals of **4** were obtained in a 32% yield based on Cu. Elemental analysis results for $C_{16}H_{21}AsCu_2Mo_3N_6O_{12}$: Calcd (%): C 19.63, H 2.16, N 8.58, Cu 12.98, Mo 29.39; Found (%): C 19.61, H 2.19, N 8.91, Cu 12.76, Mo 29.55. FTIR (KBr pellet, cm^{-1}): 1529(m), 1474(m), 1435(m), 1298(m), 1200(m), 1143(m), 1047(m), 992(m), 943(w), 891(w), 796(w), 649(w), 583(w), 517(m).

RESULTS AND DISCUSSION

The building block $[Mo_6O_{18}(O_3AsPh)_2]^{4-}$ (shortened as As_2Mo_6) in compounds **1**–**4** is similar to the α-$[Mo_8O_{26}]^{4-}$ configuration which consists of a ring of *cis*-edge sharing $\{MoO_6\}$ octahedron, capped on both faces by a $\{O_3AsPh\}$ tetrahedron. Each arsonate subunit shares three oxo-groups with the molybdate ring. In turn, each of the oxo-groups adopts the μ_3 bridging mode, linking two molybdenum atoms and one arsenic atom (Supporting Information, Figure S1).[5] The bond valence sum calculations[13] confirm that all Mo centers are in +VI oxidation states, all the As centers are in +V oxidation state, and all the Cu centers are in +I oxidation state. The As–O and Mo–O lengths are in the normal ranges.[4,14]

Structure Description of 1. Single-crystal X-ray analysis reveals that compound **1** is composed of two crystallographically independent and distinct polymeric motifs. The asymmetric unit of **1** contains one and two half Cu^{I} cations, two L1 ligands (*cis*-L1 and *trans*-L1) (Supporting Information, Figure S2), and half an As_2Mo_6 polyoxoanion (Figure 1). Cu1 cation adopts a T-type geometry, coordinated by one terminal O atom from one As_2Mo_6 polyoxoanion, and two N atoms from two *trans*-L1 ligands (Cu1–N1 = 1.885(3), Cu1–$N6^{\#1}$ = 1.881(3) and Cu1–O1 = 2.712(3) Å). Both Cu2 and Cu3 cations are two-coordinated by two nitrogen atoms from two different *cis*-L1 ligands in linear geometries (Cu2–N7 = 1.858(3) and Cu3–N12 = 1.891(3) Å). The *cis*-L1 ligands bridges neighboring Cu^{I} atoms to form the first one-dimensional (1D) S-shaped $[Cu_2(cis\text{-}L1)_2]^{2+}$ motif (Figure 2a), while the *trans*-L1 ligands and the bidentate As_2Mo_6 anions link the adjacent Cu^{I} atoms into the second two-dimensional (2D) $[(Cu1)_2(trans\text{-}L1)_2(As_2Mo_6)]^{2-}$ motif (Figure 2b). Notably, the 2D layer is highly undulated. Strikingly, the S-shaped chains penetrated into the 2D parallel layers to generate an unusual 1D + 2D → three-dimensional (3D) framework (Figures 2c and 3). From a topological viewpoint, the unusual 3D array belongs to poly*pseudo*-rotaxane architecture (Figure 3).

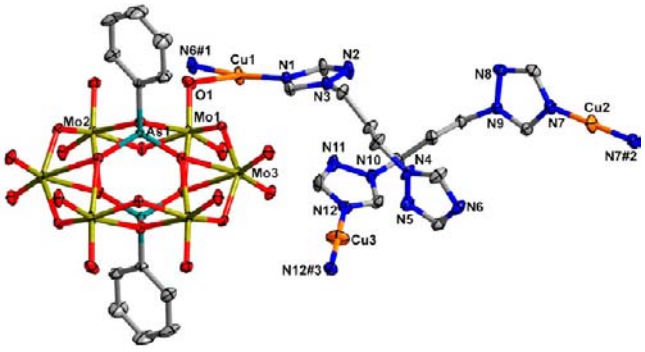

Figure 1. Coordination environments of the Cu^{I} centers in **1** with 30% thermal ellipsoids. All hydrogen atoms were omitted for clarity.

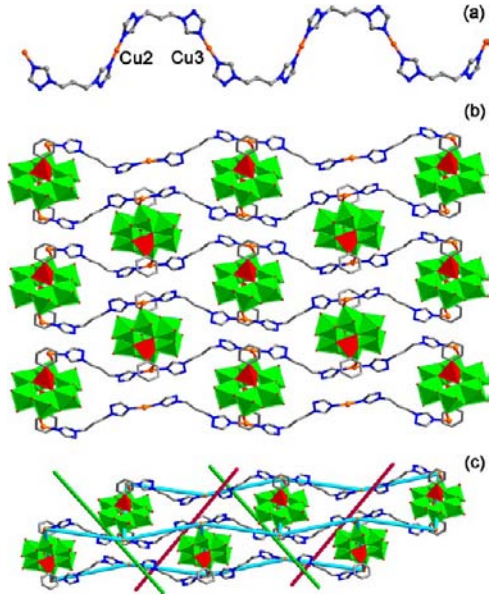

Figure 2. View of two different motifs in **1**: (a) 1D S-shaped chain, (b) 2D highly undulated layer. (c) View of the 3D poly*pseudo*-rotaxane array constructed by 1D S-shaped chains and 2D undulated layer.

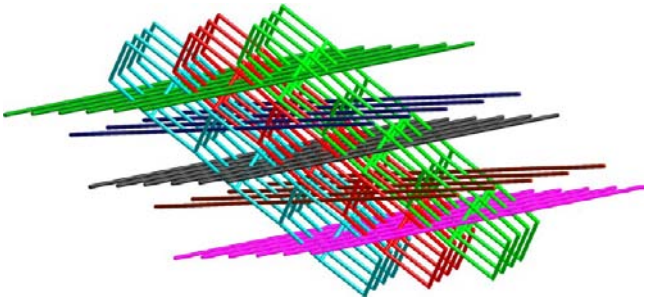

Figure 3. Schematic representation of the 3D poly*pseudo*-rotaxane framework in **1**.

It is noteworthy that the structure of **1** is different from the previously reported 3D poly*pseudo*-rotaxane architecture [Ag(bpp)][Ag_2(bpp)$_2$(ox)]NO_3 (bpp = 1,3-bis-(4-pyridyl)propane and ox = oxalate).[15] As shown in Supporting Information, Figure S3, they all show (6,3) nets; however, the detailed arrays are different. In that reported structure, each layer can be

dx.doi.org/10.1021/ic301257k | *Inorg. Chem.* 2013, 52, 84–94

considered as a honeycomb (6,3) sheet, where all atoms in one layer are almost coplanar (Supporting Information, Figure S3a). All penetrated chains are parallel to each other (Supporting Information, Figure S4). However, in **1**, the layer exhibits a wavelike brick-wall (6,3) network (Supporting Information, Figure S3b). As a result, it is penetrated by a 1D chain in two different directions (Figure 4). To the best of our knowledge, the 3D poly*pseudo*-rotaxane constructed by wavelike brick-wall (6,3) layers and 1D chains has not been reported in POM systems.[1−6]

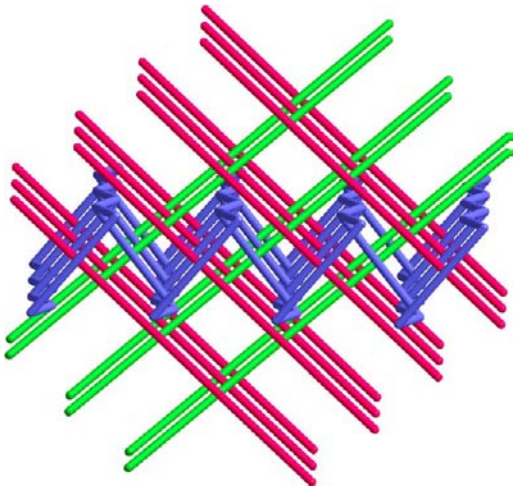

Figure 4. Schematic representation of the 1D chain penetrated in two directions in **1**.

Structure Description of 2. To investigate the influence of the spacer length of the bis(triazole) ligand on the formation of the compound structure, L2 was used under the same synthetic condition as **1**. As shown in Figure 5, the asymmetric unit of **2** contains two Cu^I cations, four half L2 ligands ($L2^a$, $L2^b$, $L2^c$, and $L2^d$, Supporting Information, Figure S5) and half an As_2Mo_6 polyoxoanion. Each Cu^I cation shows a T-type

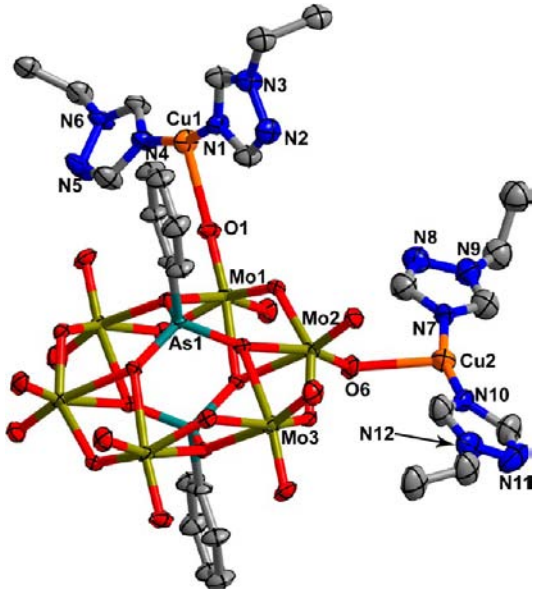

Figure 5. Coordination environments of the Cu^I centers in **2** with 30% thermal ellipsoids. All hydrogen atoms were omitted for clarity.

geometry, coordinated by one terminal O atom from one As_2Mo_6 polyoxoanion and two N atoms from two different L2 ligands (Cu1−N1 = 1.895(5), Cu1−N4 = 1.900(5), Cu2−N7 = 1.878(5), Cu2−N10 = 1.873(6), Cu1−O1 = 2.298(4), and Cu2−O6 = 2.342(4) Å). Cu1 and its symmetry-related species are bridged by $L2^a$ and $L2^b$ ligands to form a meso-helix chain (Figure 6a), while Cu2 and its symmetry-related species are

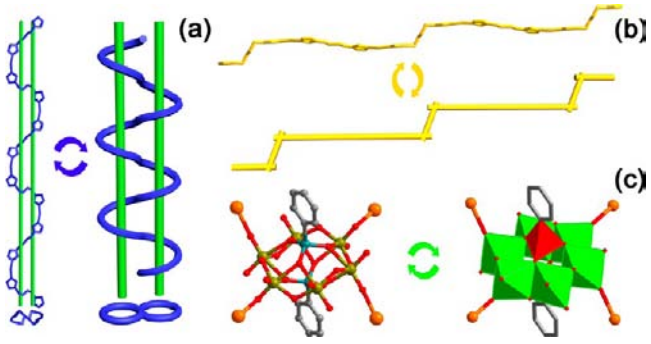

Figure 6. Three kinds of building units in **2**: (a) the meso-helix chain, (b) the stair-like chain, and (c) the tetradentate As_2Mo_6 type POM.

linked by $L2^c$ and $L2^d$ ligands to generate a stair-like chain (Figure 6b). Further, two meso-helix chains and two stair-like chains are linked by the tetradentate As_2Mo_6 polyoxoanion into an intricate 3D framework (Figures 6c, and Supporting Information, Figures S6 and S7).

From a topological viewpoint, if each Cu^I cation is considered to be a 3-connected node and each As_2Mo_6 polyoxoanion is regarded as a 4-connected node, the framework of **2** becomes a 3D trinodal (3,4)-connected net with the Point Symbol of $(8^3)_2(8^2{\cdot}12^4)$ (Figure 7). By careful inspection of the

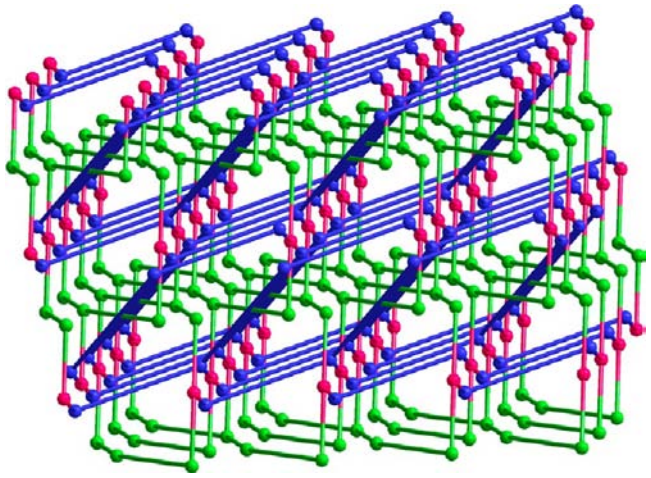

Figure 7. Schematic representation of the 3D trinodal (3,4)-connected net of **2**.

structure, we found that the framework of **2** is self-penetrating, where the rods pass through the circuits (Supporting Information, Figure S8). As far as we know, only a few POM-based self-penetrating frameworks have been reported so far.[16] However, POM-based self-penetrating (3,4)-connected framework has not been observed before.

Structure Description of 3. When a relatively long bis(triazole) ligand L3 was utilized to replace L1 under the same synthetic condition, a structurally different compound **3**

dx.doi.org/10.1021/ic301257k | *Inorg. Chem.* 2013, 52, 84−94

was obtained. As shown in Figure 8, the asymmetric unit of **3** contains two Cu^{I} cations, two L3 ligands ($L3^{a}$ and $L3^{b}$,

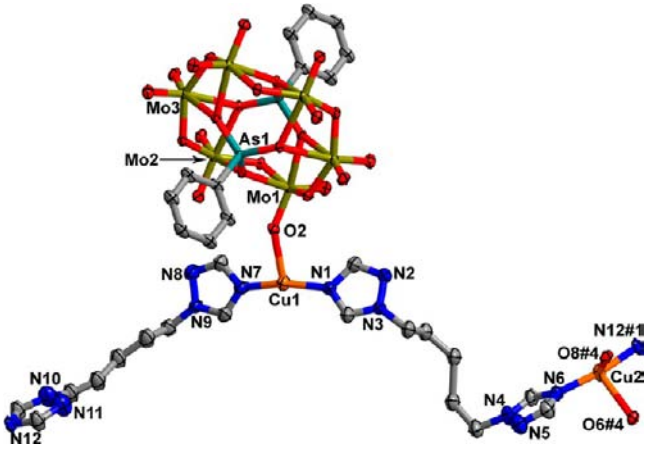

Figure 8. Coordination environments of the Cu^{I} centers of **3** with 30% thermal ellipsoids. All hydrogen atoms were omitted for clarity.

Supporting Information, Figure S9) and half an As_2Mo_6 polyoxoanion. The Cu1 cation shows a T-type geometry, defined by one terminal O atom from one As_2Mo_6 polyoxoanion and two N atoms from one $L3^{a}$ and one $L3^{b}$ ligands (Cu1−N1 = 1.876(7), Cu1−N7 = 1.881(7), and Cu1−O2 = 2.324(4) Å). The Cu2 cation adopts a "seesaw" geometry, coordinated by two terminal O atoms from one As_2Mo_6 polyoxoanion and two N atoms from one $L3^{a}$ and one $L3^{b}$ ligands (Cu2−N6 = 1.882(6), Cu2−$N12^{\#1}$ = 1.885(6), Cu2−$O6^{\#4}$ = 2.455(2), and Cu2−$O8^{\#4}$ = 2.781(6) Å). Cu1, Cu2 and their symmetry-related species are linked alternatively by $L3^{a}$ and $L3^{b}$ ligands to generate a helix chain (Supporting Information, Figure S10). Each As_2Mo_6 polyoxoanion joints four Cu^{I} cations from four parallel helix chains to yield a 2D double-layer structure (Figure 9).

Topologically, if Cu1 and Cu2 cations are considered as 3-connected nodes, respectively, and the As_2Mo_6 polyoxoanion acts as a 4-connected node, the 2D double-layer can be regarded as a trinodal (3,4)-connected network with $(6^2{\cdot}8)_2(6^2{\cdot}8^4)$ topology (Figure 10a). The most fascinating and peculiar structural feature of **3** is that each double-layer is interlocked by the two nearest neighboring ones to form a 3D polycatenated framework (Figure 10b). It is well-known that the polycatenated features have been widely reported in coordination polymer systems. However, the POM-based polycatenated framework is not common, and POM-based

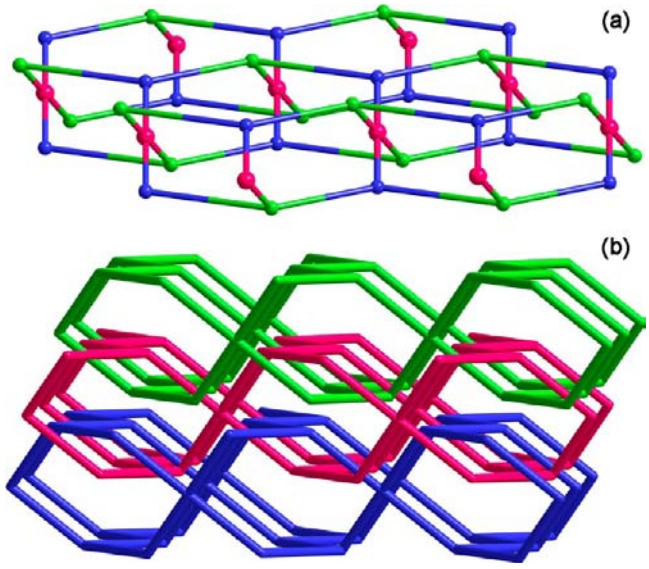

Figure 10. (a) Schematic representation of the trinodal (3,4)-connected net of **3**, and (b) view of the 2D→3D polycatenated framework.

compound with polycatenated feature similar to compound **3** has never been reported so far.[1−6]

Structure Description of 4. When a longer bis(triazole) ligand L4 was employed to replace L1 under the same synthetic condition, a new compound **4** was obtained. As shown in Figure 11, the asymmetric unit of **4** has two Cu^{I} cations, one L4

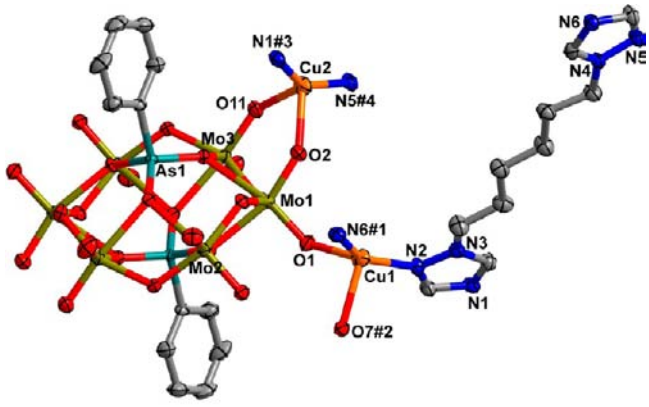

Figure 11. Coordination environments of the Cu^{I} centers in **4** with 50% thermal ellipsoids. All hydrogen atoms were omitted for clarity.

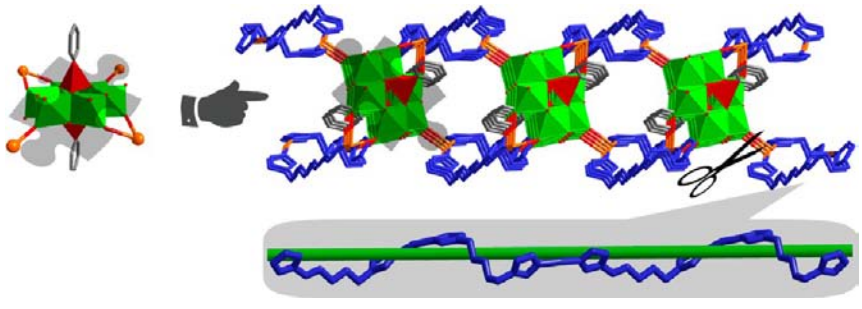

Figure 9. View of the 2D double-layer structure of **3**.

dx.doi.org/10.1021/ic301257k | *Inorg. Chem.* 2013, 52, 84−94

ligand and half an As_2Mo_6 polyoxoanion. Both Cu1 and Cu2 cations show the "seesaw" geometries. Cu1 cation is coordinated by two terminal O atoms from two As_2Mo_6 polyoxoanions and two N atoms from two adjacent L4 ligands (Cu1−N2 = 1.968(3), Cu1−N6$^{\#1}$ = 1.961(3), Cu1−O1 = 2.211(2), and Cu1−O7$^{\#2}$ = 2.238(2) Å), while Cu2 cation is coordinated by two terminal O atoms from one As_2Mo_6 polyoxoanion and two N atoms from two different L4 ligands (Cu2−N1$^{\#3}$ = 1.949(3), Cu2−N5$^{\#4}$ = 1.966(3), Cu2−O2 = 2.237(2), and Cu2−O11 = 2.181(2) Å). Notably, in **4**, L4 ligand shows one kind of configuration and coordinates with Cu^I cations in tetradentate mode (Supporting Information, Figure S11). In this way, each L4 ligand bridges Cu1 and Cu2 cations to give a wavelike layer (Figure 12). Further, the adjacent layers are linked by the As_2Mo_6 polyoxoanion in an octadentate mode to yield a 3D framework (Figure 13).

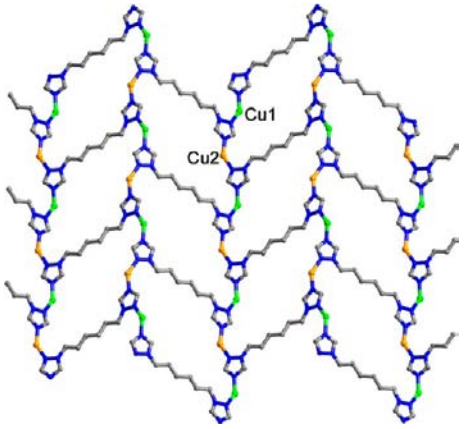

Figure 12. View of the 2D wavelike layer in **4**.

Topologically, if Cu1 and Cu2 cations are considered to be 4-connected and 3-connected nodes, respectively, L4 ligand acts as a 4-connected node, and the As_2Mo_6 polyoxoanion is considered as a 6-connected node, then the structure of compound **4** can be simplified as a 3D tetranodal (3,4,6)-connected net with the $(6^3)(4{\cdot}6^3{\cdot}8^2)(6^4{\cdot}8^2)(4^2{\cdot}6^2{\cdot}8^{10}{\cdot}10)$ topology (Figure 14). As far as we know, up to date, only one 3D trinodal (3,4,6)-connected net with the Point Symbol of $(6^3)(6^5{\cdot}8)(6^{12}{\cdot}8{\cdot}10^2)$ has been reported in compound $[Co_2(Hbidc)_2(bpt)_2]{\cdot}7H_2O$ (H_3bidc = 1*H*-benzimidazole-5,6-dicarboxylic acid, bpt = 1*H*-3,5-bis(4-pyridyl)-1,2,4-triazole).[17] However, the 3D tetranodal (3,4,6)-connected polyoxometalate-based framework has never been observed in coordination chemistry.

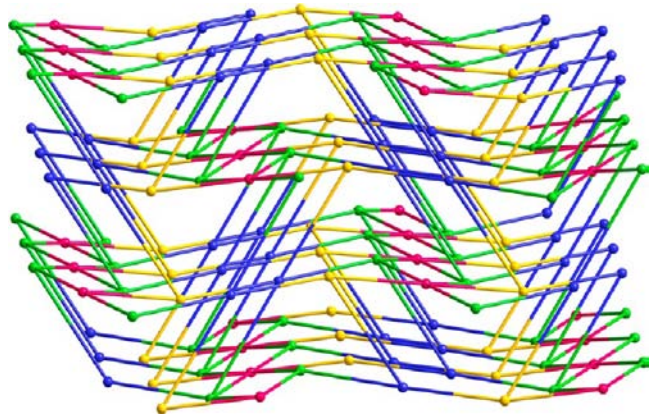

Figure 14. Schematic representation of the tetranodal (3,4,6)-connected net of **4**.

From the structure descriptions above, we can see that the introduction of the As_2Mo_6 cluster into the MOFs significantly enriched the final compound structures. Compared with the corresponding POM-free system, the introduction of the As_2Mo_6 cluster can vary the configurations and coordination modes of the bis(triazole) ligands (L1−L4). Take compounds $[Cu^I_2(cis\text{-}L1)_2][Cu^I_2(trans\text{-}L1)_2Mo_6O_{18}(O_3AsPh)_2]$ (**1**), $[Cu^I_4(L2)_4Mo_6O_{18}(O_3AsPh)_2]$ (**2**), and $[Cu^I_4(L4)_2Mo_6O_{18}(O_3AsPh)_2]$ (**4**) for example. In the reported POM-free compound $[Zn_2(HL)_2(cis\text{-}L1)_2]{\cdot}2H_2O$ (**5**) (H_3L = 5-(benzonic-4-ylmethoxy) isophthalic acid), two L1 ligands bridge adjacent Zn^{II} atoms in *cis*-configurations (Supporting Information, Figure S12) to give a dimeric unit $[Zn(L1)_2Zn]$,[18] which are further linked by HL anions to furnish a 1D ribbon structure. However, in **1**, the L1 ligands show *cis*- and *trans*-configurations (Supporting Information, Figure S2). The S-shaped $[Cu_2(cis\text{-}L1)_2]^{2+}$ chains penetrated into the 2D parallel $[(Cu1)_2(trans\text{-}L1)_2(As_2Mo_6)]^{2-}$ layers to generate an unusual 1D + 2D → 3D framework. In the reported POM-free compound $[Cu_2(L2)_{3.5}(C4AS)(H_2O)]{\cdot}2.5(H_2O)$ (**6**) (C4AS = *p*-sulfonato-calix[4]arene) (Supporting Information, Figure S13), the L2 ligands link the Cu^{II} atoms in *cis*- and *trans*-configurations to generate a 3D framework.[19] Nevertheless, in

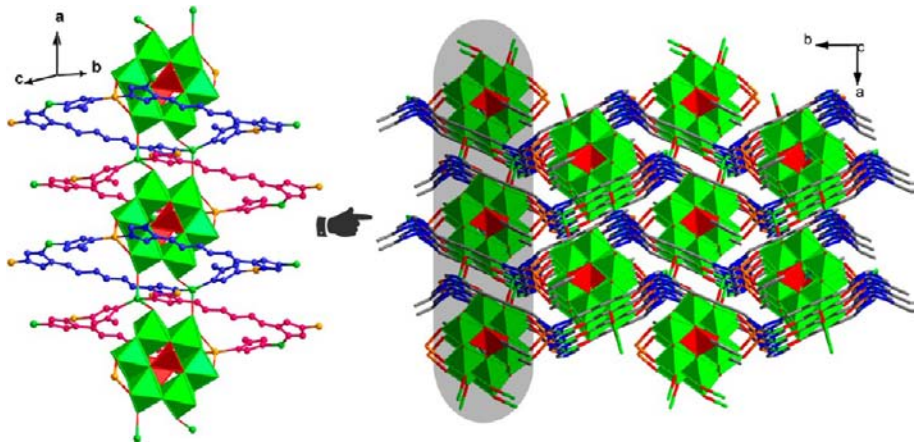

Figure 13. View of the 3D framework of **4** formed by infinite chains and parallel layers.

dx.doi.org/10.1021/ic301257k | *Inorg. Chem.* 2013, 52, 84−94

2, the Cu^I atoms are linked by the L2 ligands in *trans*-configurations (Supporting Information, Figure S5) and the As_2Mo_6 polyoxoanions in tetradentate modes, yielding a rare 3D trinodal (3,4)-connected self-penetrated framework. In addition, the effect of the introduction of the As_2Mo_6 cluster on the complex structure is also supported by the different coordination modes of the bis(triazole) ligands. For example, in the reported POM-free compound $[Zn(HL)(L4)_{0.5}]$ (**7**), neighboring Zn^{II} atoms are linked by HL anions to generate 2D layers, which are further linked by L4 in a bidentate mode (Supporting Information, Figure S14) to form a 3D (3,4)-connected framework.[18] However, in $[Cu^I_4(L4)_2Mo_6O_{18}(O_3AsPh)_2]$ (**4**), each L4 ligand bridges four Cu^I atoms in a tetradentate mode (Supporting Information, Figure S11) to yield 2D wavelike layers, which are further linked by the octadentate As_2Mo_6 polyoxoanions into a 3D tetranodal (3,4,6)-connected framework. Clearly, the introduction of the As_2Mo_6 cluster into the MOFs results in the structure differences of the compounds through the variations of the bis(triazole) ligands in the configurations and coordination modes.

Effects of the Bis(triazole) Ligands on the Frameworks. From the structure descriptions above, we can see that the bis(triazole) ligands have a remarkable effect on the construction of the final structures. In this work, four bis(triazole) ligands (L1−L4) were used to investigate the spacer length effects of the ligands on the structures. Compared with L1, L2 has an additional $-CH_2-$ group at the center of the molecule. The difference in the numbers of the $-CH_2-$ groups between L1 and L2 led to the difference in their complex structures. In **1**, the *cis*-L1 ligands bridge neighboring Cu2 and Cu3 atoms to yield a 1D S-shaped chain, whereas the *trans*-L1 ligands and As_2Mo_6 polyoxoanions link adjacent Cu1 atoms to form a highly undulated layer. Further, the S-shaped chains penetrated through the 2D parallel layers to generate an unusual 1D + 2D → 3D poly*pseudo*-rotaxane architecture. In **2**, the L2 ligands link the neighboring Cu^I atoms to furnish a −L2−Cu−L2− chains. The neighboring chains are further linked by the tetradentate As_2Mo_6 polyoxoanions to produce a rare 3D trinodal (3,4)-connected self-penetrating framework with Point Symbol of $(8^3)_2(8^2{\cdot}12^4)$. The spacer length effect on the structures was also supported by compounds **3** and **4**. Compared with L3, L4 has a relatively long alkyl spacer. In **3**, each L3 ligand bridges two Cu^I cations to generate a helix chain. The chains are further extended by As_2Mo_6 polyoxoanions into a 3D polycatenated PMOFs. In **4**, each L4 ligand links four Cu^I cations to yield a wavelike layer. The layers are further linked by As_2Mo_6 polyoxoanions to furnish a 3D tetranodal (3,4,6)-connected framework. Clearly, the spacer lengths of the bis(triazole) ligands show important effects on the structures of the PMOFs.

Coordination Modes of As_2Mo_6 Polyoxoanion. It is well-known that the POMs play an important role in both the structural diversities and the potential applications of the compounds.[1−3] The POMs can coordinate with metals in various modes, leading to structural diversities of the final compounds. As shown in Figure 15, the As_2Mo_6 polyoxoanions in **1**−**4** adopt four different coordination fashions (bidentate, tetradentate, hexadentate, and octadentate modes), which have significant effects on the final structures of the compounds. In **1**, the As_2Mo_6 polyoxoanion in a bidentate mode coordinated with two Cu^I cations through two terminal O atoms (Figure 15a). The bidentate As_2Mo_6 anions and the *trans*-L1 ligands

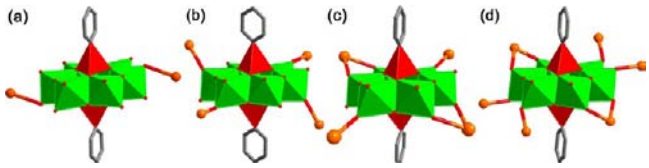

Figure 15. Coordination modes of As_2Mo_6 polyoxoanions.

link the adjacent Cu^I atoms to form the 2D $[(Cu1)_2(trans\text{-}L1)_2(As_2Mo_6)]^{2-}$ motif. The 2D highly undulated motifs are further penetrated by the S-shaped $[Cu_2(cis\text{-}L1)_2]^{2+}$ chains to generate an unusual 1D + 2D → 3D framework. However, in **2**, the As_2Mo_6 anion bridges four Cu^I cations in a tetradentate mode (Figure 15b). The tetradentate As_2Mo_6 polyoxoanions and the L2 ligands linked the Cu^I atoms to furnish a rare 3D trinodal (3,4)-connected self-penetrated framework. In **3**, the As_2Mo_6 polyoxoanion links four Cu^I cations with its six terminal O atoms (Figure 15c). Adjacent Cu^I atoms are linked by As_2Mo_6 polyoxoanions and L3 ligands into 2D layers, which are further interlocked by the two nearest neighboring ones to form a 3D polycatenated framework. However, in **4**, the polyoxoanion joints six Cu^I cations in an octadentate mode (Figure 15d). In this fashion, the As_2Mo_6 polyoxoanions linked the neighboring layers constructed by L4 ligands and Cu^I cations to generate a 3D tetranodal (3,4,6)-connected framework. Obviously, from the coordination behaviors of the As_2Mo_6 anions in **1**−**4**, we can see that the coordination modes and coordination numbers of the As_2Mo_6 polyoxoanions have great influence on the frameworks of the PMOFs.

Thermal Analysis and PXRD Results. To characterize the compounds more fully in terms of thermal stability, their thermal behaviors were studied by TGA. The experiments were performed on samples consisting of numerous single crystals of **1**−**4** under N_2 atmosphere with a heating rate of 10 °C/min (Supporting Information, Figure S15). The networks remain intact for these compounds until about 280 °C, and then begin to collapse. For **1**, the weight loss between 280 and 630 °C is attributed to decomposition of the organic components and As_2O_3 (obsd 48.9%, calcd 47.7%). Compound **2** loses its organic components and As_2O_3 from 270 to 800 °C (obsd 49.2%, calcd 49.0%). In the case of **3**, weight loss of 51.3% (calcd 50.2%) between 270 and 715 °C is also attributed to the organic components and As_2O_3. For **4**, the weight loss in the temperature range of 290−730 °C corresponds to the departure of organic components and As_2O_3 (obsd 41.4%, calcd 40.5%).

To confirm whether the crystal structures are truly representative of the bulk materials, PXRD experiments were carried out for **1**−**4**. The experimental PXRD patterns are in good agreement with the corresponding simulated ones (Supporting Information, Figures S16−S19) except for the relative intensity variation because of preferred orientations of the crystals.

Optical Band Gap. The UV−vis absorption spectra of compounds **1**−**4** were measured in the crystalline state at room temperature (Supporting Information, Figure S20). The energy bands from 200 to 300 nm for **1**, 200 to 320 for **2**, 200 to 300 nm for **3**, and 200 to 310 nm for **4** may be assigned to the O→Mo charge transfers.[2e]

To study the conductivity of compounds **1**−**4**, the diffuse reflectivities for powder samples were conducted to obtain their band gaps (E_g). The band gaps (E_g) were confirmed as the intersection point between the energy axis and the line

dx.doi.org/10.1021/ic301257k | *Inorg. Chem.* 2013, 52, 84−94

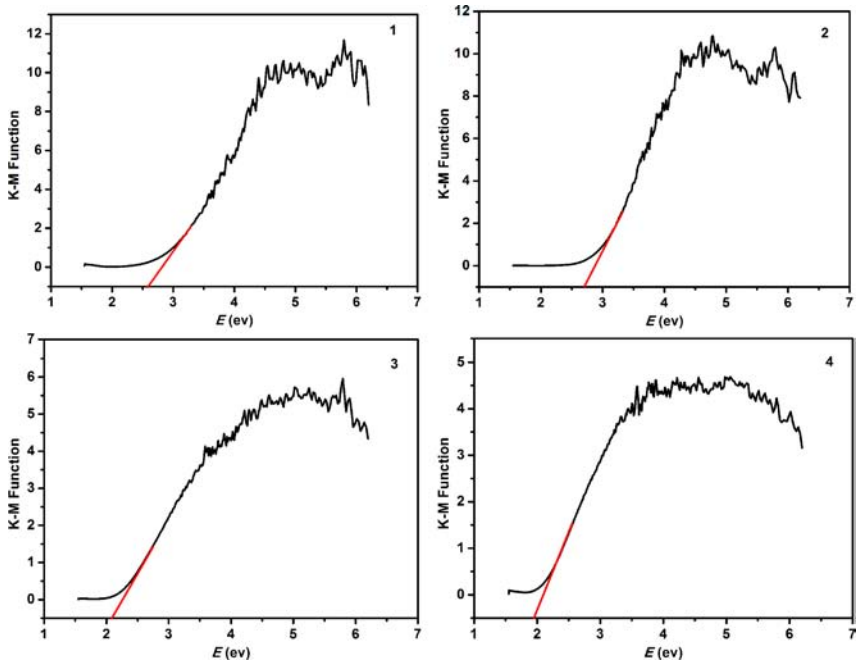

Figure 16. Kubelka–Munk-tranformed diffuse reflectance spectra of compounds **1**–**4**.

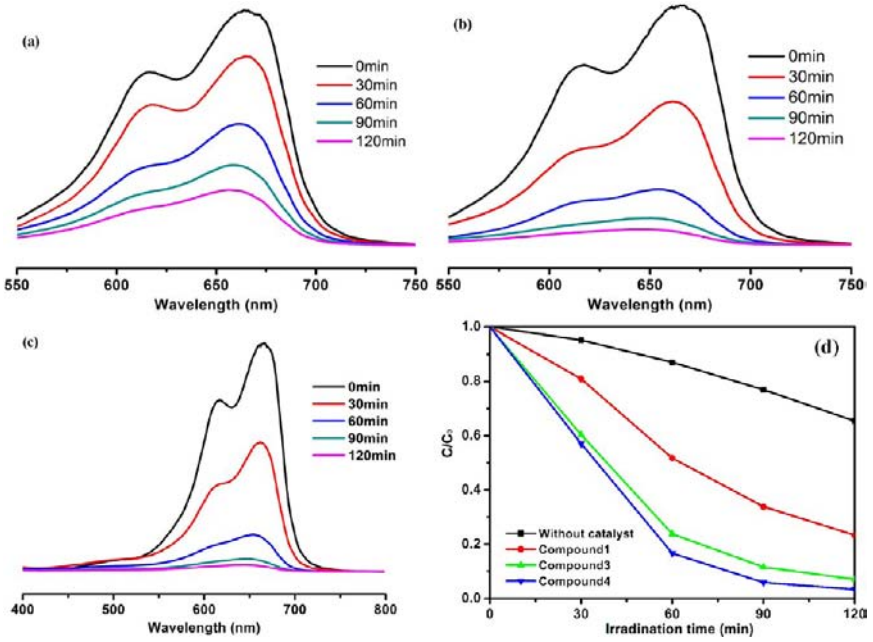

Figure 17. (a–c) UV–vis absorption spectra of the **MB** solution during the decomposition reaction under UV light irradiation in the presence of **1**, **3**, and **4**. (d) Plot of irradiation time versus concentration for **MB** under UV light in the presence of the compound **1**, **3**, and **4**, and the black curve is the control experiment without any catalyst.

extrapolated from the linear portion of the adsorption edge in a plot of the Kubelka–Munk function F against E.[20] The optical absorption related to E_g can be assessed at 2.6 eV for **1**, 2.7 eV for **2**, 2.1 eV for **3**, and 1.9 eV for **4**, respectively (Figure 16). The reflectance spectra show the presence of optical band gaps and the nature of semiconductivities for compounds **1**–**4**. Thus, compounds **1**–**4** have potential for photocatalytic activities.[2]

Photocatalysis Properties. Photocatalytic properties of POMs have attracted much attention because of their potential applications in purifying air and water.[21−24] The introduction of POMs into MOFs can enrich their potential applications, such as catalysis, nonlinear optics, and electrical conductivity.[1−3] Herein, compounds **1**, **3**, and **4** have been tested for photocatalytic degradation of **MB**.[25] The experimental details have been described in our previous work.[2e] In a typical experiment, a 200 mL **MB** (5.0×10^{-5} mol L^{-1}) solution was taken along with the catalyst (**1**, **3**, and **4**) (70 mg) and exposed to UV light. As illustrated in Figure 17, the concentrations of **MB** versus irradiation time of **1**, **3**, and **4** were plotted. It can be seen that the photocatalytic activities increase from 35% (without catalysts) to 76% for **1**, 93% for **3**, and 97% for **4** after

dx.doi.org/10.1021/ic301257k | Inorg. Chem. 2013, 52, 84−94

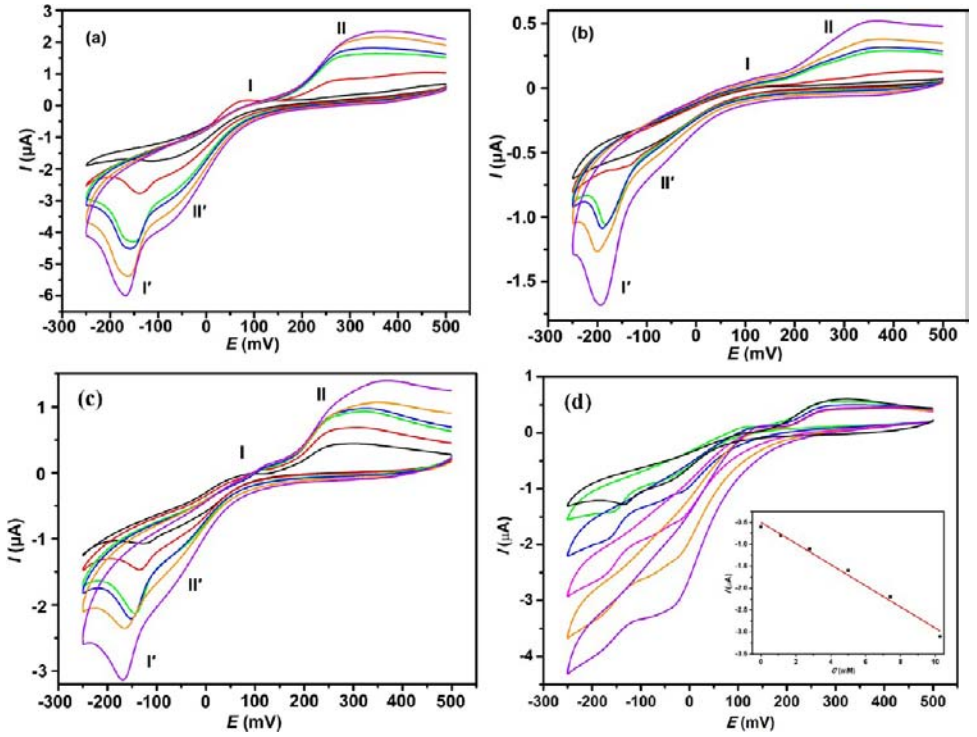

Figure 18. (a) Cyclic voltammograms of the **1**-CPE, (b) **4**-CPE, and (c) **3**-CPE in 1 M H_2SO_4 at different scan rates (from inner to outer: 20, 40, 60, 100, 150, and 200 mV·s^{-1}). (d) Cyclic voltammograms of the **3**-CPE in 1 M H_2SO_4 containing 0.0, 1.1, 2.8, 5.0, 7.4, and 10.3 mM $NaNO_2$. Scan rate: 40 mV·s^{-1}. Inset: the variation of cathodic peak currents vs $NaNO_2$ concentrations.

120 min of irradiation. Obviously, the degradation efficiency of **4** under UV light is higher than those of **1** and **3.** In ref 22b, the concentration of the **MB** solution is 2.7×10^{-5} mol L^{-1} and the volume of the solution is 90 mL. Compared with ref 22b, we used the UV mercury lamp with the same power (125 W) and **MB** solution with higher concentration (5.0×10^{-5} mol L^{-1}). After 90 min of irradiation, the photocatalytic activity increased from 24% (without catalysts) to 66% for **1**, 88% for **3**, and 94% for **4** (Figure 17d). It shows that the photocatalytic activity for **1** is similar to that reported by ref 22b (ca. 70%), while for **3** and **4**, the photocatalytic activities are much higher than that reported by ref 22b. These results demonstrate that compounds **1**, **3**, and **4** may be good potential photocatalysts with photocatalytic activities in the degradation of some organic dyes.

Generally, the POM subunit is regarded as the photocatalytic active component for the PMOFs.[22] Therefore, the photocatalytic activities for the PMOFs are mainly dependent on their POM-containing structures. Notably, although **1**, **3**, and **4** show the overall 3D structures, the extended As_2Mo_6-containing structure of **1** is entirely different from that of **3** or **4**. Compound **1** contains the only 2D As_2Mo_6-containing layer ($[(Cu1)_2(trans\text{-}L1)_2(As_2Mo_6)]^{2-}$). However, in **3** and **4**, the As_2Mo_6-containing structures show the 3D polycatenated framework and the 3D tetranodal (3,4,6)-connected framework, respectively. Obviously, in **3** and **4**, the photocatalytic active As_2Mo_6 polyoxoanions distribute overall the 3D framework. The photocatalytic results of **1**, **3**, and **4** indicate that the more extended 3D As_2Mo_6-containing frameworks of **3** and **4** have an advantage over the 2D As_2Mo_6-containing layer of **1** during the photocatalytic decomposition reaction with **MB**. In other words, the more extended As_2Mo_6-containing frameworks of **3** and **4** favor the transport of excited holes/electrons to the surfaces to initiate the photocatalytic decomposition reaction with **MB**.[22a]

The photostabilities of **1**, **3**, and **4** were monitored by using PXRD experiments. After photocatalysis, the experimental PXRD patterns are also nearly identical to that of the original compounds, which confirmed that their stability toward photocatalysis is good (Supporting Information, Figures S16–S19.

Cyclic Voltammetry. Redox properties of compounds **1**, **3**, and **4** were studied in 1 M H_2SO_4 aqueous solution. The electrochemical behaviors of the **1**-, **3**-, and **4**-CPE (Figure 18) are similar except for some slight potential shift, and the behavior of **3**-CPE has been taken as an example.[26] The cyclic voltammograms for **3**-CPE at different scan rates are presented in Figure 18c in the potential range of −250 to 500 mV. There exist two reversible redox peaks I–I′ and II–II′ with the half-wave potentials $E_{1/2}$ [= $(E_{pa} + E_{pc})/2$] at −28(I–I′) and 279(II–II′) mV (scan rate: 40 mV·s^{-1}), respectively. The redox peaks I–I′ and II–II′ might be ascribed to the As_2Mo_6 cluster. When the scan rates were varied from 20 to 200 mV·s^{-1}, the peak potentials change gradually: the cathodic peak potentials shift slightly toward negative potential values and the corresponding anodic peak potentials shift toward positive potential values with increasing scan rates.[27]

The **3**-CPE presents electrocatalytic activity for the reduction of nitrite, as shown in Figure 18d. With the addition of nitrite, all two reduction peak currents gradually increase while the corresponding oxidation peak currents decrease, suggesting that nitrite is reduced. The inset of Figure 18d shows that catalytic currents were linear with $NaNO_2$ concentration up to 10.5 mM.

dx.doi.org/10.1021/ic301257k | Inorg. Chem. 2013, 52, 84–94

CONCLUSIONS

In summary, four novel PMOFs based on As_2Mo_6 building blocks and copper(I)-organic fragments have been synthesized under the similar synthetic conditions. The series of PMOFs display fascinating 3D frameworks with poly*pseudo*-rotaxane, self-penetrated and polycatenated features. The successful isolation of these solid materials provides intriguing examples of entangled architectures. It has been proven that the bis(triazole) ligands and As_2Mo_6 building blocks are good candidates for the construction of PMOFs with diverse structures. The photocatalytic behaviors of compounds **1**, **3**, and **4** indicate they are good and stable photocatalysts for the photodegradation of **MB** under UV light. Their electrochemical studies show that the **3**-CPE presents electrocatalytic activity for the reduction of nitrite.

ASSOCIATED CONTENT

Supporting Information

Crystallographic data in CIF format. Further details are given in Figures S1−S20 and Tables S1−S4. This material is available free of charge via the Internet at http://pubs.acs.org.

AUTHOR INFORMATION

Corresponding Author

*E-mail: yangjinnenu@yahoo.com.cn (J.Y.), jianfangma@yahoo.com.cn (J.-F.M.). Fax: +86-431-85098620 (J.-F.M.).

Notes

The authors declare no competing financial interest.

ACKNOWLEDGMENTS

We thank the National Natural Science Foundation of China (Grant No. 21071028, 21001023), the Science Foundation of Jilin Province (201215005, 20100109), the Fundamental Research Funds for the Central Universities, the Specialized Research Fund for the Doctoral Program of Higher Education, the Training Fund of NENU's Scientific Innovation Project and the Analysis and Testing Foundation of Northeast Normal University for support.

REFERENCES

(1) (a) Long, D. L.; Burkholder, E.; Cronin, L. *Chem. Soc. Rev.* **2007**, *36*, 105. (b) Rosnes, M. H.; Musumeci, C.; Pradeep, C. P.; Mathieson, J. S.; Long, D. L.; Song, Y. F.; Pignataro, B.; Cogdell, R.; Cronin, L. *J. Am. Chem. Soc.* **2010**, *132*, 15490. (c) Cooper, G. J. T.; Boulay, A. G.; Kitson, P. J.; Ritchie, C.; Richmond, C. J.; Thiel, J.; Gabb, D.; Eadie, R.; Long, D. L.; Cronin, L. *J. Am. Chem. Soc.* **2011**, *133*, 5947. (d) Wu, H.; Yang, J.; Su, Z. M.; Batten, S. R.; Ma, J. F. *J. Am. Chem. Soc.* **2011**, *133*, 11406.

(2) (a) Dolbecq, A.; Dumas, E.; Mayer, C. R.; Mialane, P. *Chem. Rev.* **2010**, *110*, 6009. (b) Xu, L.; Lu, M.; Xu, B. B.; Wei, Y. G.; Peng, Z. H.; Powell, D. R. *Angew. Chem., Int. Ed.* **2002**, *41*, 4129. (c) Kögerler, P.; Cronin, L. *Angew. Chem., Int. Ed.* **2005**, *44*, 844. (d) Chen, L.; Jiang, F. L.; Lin, Z. Z.; Zhou, Y. F.; Yue, C. Y.; Hong, M. C. *J. Am. Chem. Soc.* **2005**, *127*, 8588. (e) Liu, B.; Yu, Z. T.; Yang, J.; Hua, W.; Liu, Y. Y.; Ma, J. F. *Inorg. Chem.* **2011**, *50*, 8967.

(3) (a) Sun, C. Y.; Liu, S. X.; Liang, D. D.; Shao, K. Z.; Ren, Y. H.; Su, Z. M. *J. Am. Chem. Soc.* **2009**, *131*, 1883. (b) An, H. Y.; Wang, E. B.; Xiao, D. R.; Li, Y. G.; Su, Z. M.; Xu, L. *Angew. Chem., Int. Ed.* **2006**, *45*, 904. (c) Lan, Y. Q.; Li, S. L.; Wang, X. L.; Shao, K. Z.; Su, Z. M.; Wang, E. B. *Inorg. Chem.* **2008**, *47*, 529.

(4) (a) Zheng, S. T.; Zhang, J.; Li, X. X.; Fang, W. H.; Yang, G. Y. *J. Am. Chem. Soc.* **2010**, *132*, 15102. (b) Song, Y. F.; McMillan, N.; Long, D. L.; Kane, S.; Malm, J.; Riehle, M. O.; Pradeep, C. P.; Gadegaard, N.; Cronin, L. *J. Am. Chem. Soc.* **2009**, *131*, 1340. (c) Mizuno, N.; Yamaguchi, K.; Kamata, K. *Coord. Chem. Rev.* **2005**, *249*, 1944. (d) Zhu, Y. L.; Wang, L. S.; Zhao, J.; Yin, P. C.; Zhang, J.; Li, Q.; Zhu, L.; We, Y. G. *Chem.—Eur. J.* **2009**, *15*, 3076. (e) Liu, H. Y.; Liu, B.; Yang, J.; Liu, Y. Y.; Ma, J. F.; Wu, H. *Dalton Trans.* **2011**, *40*, 9782.

(5) (a) Finn, R. C.; Burkholder, E.; Zubieta, J. *Chem. Commun.* **2001**, 1852. (b) Burkholder, E.; Golub, V.; O'Connor, C. J.; Zubieta, J. *Chem. Commun.* **2003**, 2128. (c) Finn, R. C.; Rarig, R. S.; Zubieta, J. *Inorg. Chem.* **2002**, *41*, 2190. (d) Armatas, N. G.; Allis, D. G.; Prosvirin, A.; Carnutu, G.; O'Connor, C. J.; Dunbar, K.; Zubieta, J. *Inorg. Chem.* **2008**, *47*, 832. (e) Zheng, S. T.; Zhang, J.; Yang, G. Y. *Angew. Chem., Int. Ed.* **2008**, *47*, 3909. (f) Liu, H. Y.; Wu, H.; Ma, J. F.; Liu, Y.-Y.; Yang, J.; Ma, J. C. *Dalton Trans.* **2011**, *40*, 602.

(6) (a) Kwak, W.; Rajkovic, L. M.; Stalick, J. K.; Pope, M. T.; Quicksall, C. O. *Inorg. Chem.* **1976**, *15*, 2778. (b) Burkholder, E.; Wright, S.; Golub, V.; O'Connor, C. J.; Zubieta, J. *Inorg. Chem.* **2003**, *42*, 7460. (c) Tian, A. X.; Ying, J.; Peng, J.; Sha, J. Q.; Pang, H. J.; Zhang, P. P.; Chen, Y.; Zhu, M.; Su, Z. M. *Cryst. Growth Des.* **2008**, *8*, 3717. (d) Zheng, S. T.; Yang, G. Y. *Dalton Trans.* **2010**, *39*, 700. (e) Ren, Y. P.; Kong, X. J.; Hu, X. Y.; Sun, M.; Long, L. S.; Huang, R. B.; Zheng, L. S. *Inorg. Chem.* **2006**, *45*, 4016.

(7) (a) Tian, A. X.; Ying, J.; Peng, J.; Sha, J. Q.; Han, Z. G.; Ma, J. F.; Su, Z. M.; Hu, N. H.; Jia, H. Q. *Inorg. Chem.* **2008**, *47*, 3274. (b) Tian, A. X.; Ying, J.; Peng, J.; Sha, J. Q.; Pang, H. J.; Zhang, P. P.; Chen, Y.; Zhu, M.; Su, Z. M. *Inorg. Chem.* **2009**, *48*, 100.

(8) (a) Wang, X. L.; Qin, C.; Wang, E. B.; Su, Z. M. *Chem. Commun.* **2007**, 4245. (b) Wang, X. L.; Qin, C.; Wang, E. B.; Su, Z. M.; Li, Y. G.; Xu, L. *Angew. Chem., Int. Ed.* **2006**, *45*, 7411.

(9) Albada, G. A. V.; Guijt, R. C.; Haasnoot, J. G.; Lutz, M.; Spek, A. L.; Reedijk, J. *Eur. J. Inorg. Chem.* **2000**, 121.

(10) Sheldrick, G. M. *SHELXS-97, Programs for X-ray Crystal Structure Solution*; University of Göttingen: Göttingen, Germany, 1997.

(11) Sheldrick, G. M. *SHELXL-97, Programs for X-ray Crystal Structure Refinement*; University of Göttingen: Göttingen, Germany, 1997.

(12) Farrugia, L. J. *WINGX, A Windows Program for Crystal Structure Analysis*; University of Glasgow, Glasgow, U.K., 1988.

(13) Brown, I. D.; Altermatt, D. *Acta Crystallogr.* **1985**, *B41*, 244.

(14) (a) Kwak, W.; Rajkovic, L. M.; Pope, M. T.; Quicksall, C. O.; Matsumoto, K. Y.; Sasaki, Y. *J. Am. Chem. Soc.* **1977**, *99*, 6463. (b) Hedman, B. *Acta Crystallogr.* **1980**, *B36*, 2241.

(15) Tong, M. L.; Wu, Y. M.; Ru, J.; Chen, X. M.; Chang, H.; Kitagawa, S. *Inorg. Chem.* **2002**, *41*, 4846.

(16) (a) Qu, X. S.; Xu, L.; Gao, G. G.; Li, F. Y.; Yang, Y. Y. *Inorg. Chem.* **2007**, *46*, 4775. (b) Lan, Y. Q.; Li, S. L.; Wang, X. L.; Shao, K. Z.; Du, D. Y.; Su, Z. M.; Wang, E. B. *Chem.—Eur. J.* **2008**, *14*, 9999.

(17) Huang, F. P.; Tian, J. L.; Li, D. D.; Chen, G. J.; Gu, W.; Yan, S. P.; Liu, X.; Liao, D. Z.; Cheng, P. *CrystEngComm* **2010**, *12*, 395.

(18) Liu, Y. Y.; Li, J.; Ma, J. F.; Ma, J. C.; Yang, J. *CrystEngComm* **2012**, *14*, 169.

(19) Chen, C.; Ma, J. F.; Liu, B.; Yang, J.; Liu, Y. Y. *Cryst. Growth Des.* **2011**, *11*, 4491.

(20) (a) Pankove, J. I. *Optical Processes in Semiconductors*; Prentice Hall: Englewood Cliffs, NJ, 1971. (b) Wesley, W. M.; Harry, W. G. H. *Reflectance Spectroscopy*; Wiley: New York, 1966.

(21) Dong, M. Y.; Lin, Q.; Su, H. M.; Chen, D.; Zhang, T.; Wu, Q. Z.; Li, S. P. *Cryst. Growth Des.* **2011**, *11*, 5002.

(22) (a) Lin, H.; Maggard, P. A. *Inorg. Chem.* **2008**, *47*, 8044. (b) Hu, Y.; Luo, F.; Dong, F. F. *Chem. Commun.* **2011**, *47*, 761. (c) Wu, Q.; Chen, W. L.; Liu, D.; Liang, C.; Li, Y. G.; Lin, S. W.; Wang, E. B. *Dalton Trans.* **2011**, *40*, 56.

(23) (a) Guo, Y. H.; Wang, Y. H.; Hu, C. W.; Wang, Y. H.; Wang, E. B.; Zhou, Y. C.; Feng, S. H. *Chem. Mater.* **2000**, *12*, 3501. (b) Mylonas, A.; Hiskia, A.; Papaconstanitinou, E. *J. Mol. Catal. A: Chem.* **1996**, *114*, 191.

(24) Mylonas, A.; Papacontantinous, E. *J. Photochem. Photobiol. A* **1996**, *94*, 77.

(25) (a) Yu, Z. T.; Liao, Z. L.; Jiang, Y. S.; Li, G. H.; Chen, J. S. *Chem.—Eur. J.* **2005**, *11*, 2642. (b) Liao, Z. L.; Li, G. D.; Bi, M. H.; Chen, J. S. *Inorg. Chem.* **2008**, *47*, 4844.

(26) Han, Z. G.; Zhao, Y. L.; Peng, J.; Liu, Q.; Wang, E. B. *Electrochim. Acta* **2005**, *51*, 218.
(27) (a) Wang, B. X.; Dong, S. J. *Electrochim. Acta* **1992**, *37*, 1859. (b) Wang, P.; Wang, X. P.; Zhu, G. Y. *Electrochim. Acta* **2000**, *46*, 637. (c) Dong, S. J.; Wang, B. X. *Electrochim. Acta* **1992**, *37*, 11.